Observationally Verifiable Predictions of Modified Gravity

J. W. Moffat

Perimeter Institute For Theoretical Physics,

Waterloo, Ontario, Canada

Talk given at the conference The Invisible Universe,
Paris, June 29-July 3, 2009

1. Introduction

• A fully relativistic modified gravity (MOG) called Scalar-Tensor-Vector-Gravity (STVG) (JWM, JCAP 2006, 004 (2006), arXiv:gr-qc/0506021) can be derived from an action principle. It leads to a self-consistent, stable gravity theory that can describe solar system, astrophysical and cosmological data.

• The STVG theory has an extra degree of freedom, a vector field called a "phion" field whose curl is a skew field that couples to matter ("fifth force"). The gravitational field is described by a symmetric Einstein metric tensor.

• The modified gravity theory is not Milgrom's MOND (1983) or Bekenstein's TeVeS (2004). I call it MOG (modified gravity).

•The classical theory allows the gravitational coupling "constant" G to vary as a scalar field with space and time. The effective mass of the skew symmetric field and the coupling of the field to matter also vary with space and time as scalar fields.

- The modified Newtonian acceleration law for weak fields can fit a large amount of galaxy rotation curve data without non-baryonic dark matter. It also can fit data for X-ray galaxy clusters without dark matter. The modified acceleration law is consistent with the solar system data (J. R. Brownstein and JWM, 2006; JWM & V. T. Toth, 2007, 2008; J. R. Brownstein, 2008).

The MOG must also explain the following:

- The CMB data including the power spectrum data;
- The formation of proto-galaxies in the early universe and the growth of galaxies;
- Gravitational lensing data for galaxies and clusters of galaxies;
- The Bullet Cluster 1E0-657-56 and the merging clusters Abell 520 and MACS J0025.4 – 1222;
- N-body simulations of galaxy surveys;
- The accelerating expansion of the universe.

2. Modified Gravity (MOG)

- The Scalar-Tensor-Vector-Gravity (STVG) action takes the form:

$$S = S_G + S_\varphi + S_S + S_M.$$

$$S_G = -\frac{1}{16\pi}\int \frac{1}{G}\left(R + 2\Lambda\right)\sqrt{-g}\,d^4x,$$

$$S_\phi = -\int \omega\left[\frac{1}{4}B^{\mu\nu}B_{\mu\nu} - \frac{1}{2}\mu^2\phi_\mu\phi^\mu + V_\phi(\phi)\right]\sqrt{-g}\,d^4x,$$

$$S_S = -\int \frac{1}{G}\left[\frac{1}{2}g^{\mu\nu}\left(\frac{\nabla_\mu G\nabla_\nu G}{G^2} + \frac{\nabla_\mu\mu\nabla_\nu\mu}{\mu^2} - \nabla_\mu\omega\nabla_\nu\omega\right) + \frac{V_G(G)}{G^2} + \frac{V_\mu(\mu)}{\mu^2} + V_\omega(\omega)\right]\sqrt{-g}\,d^4x.$$

- In addition to the metric $g_{\mu\nu}(x)$, we have a massive vector field $\varphi_\mu(x)$, and 3 scalar fields $G(x)$, $\omega(x)$ and $\mu(x)$. $B_{\mu\nu} = \partial_\mu\varphi_\nu - \partial_\nu\varphi_\mu$ and $V_\varphi(\varphi)$, $V_G(G)$, $V_\omega(\omega)$ and $V_\mu(\mu)$ denote self-interaction potentials.

• The field equations have exact numerical solutions given initial values for the field quantities and boundary conditions (JWM and V. T. Toth, 2007, 2009, Class. and Quant. Grav. 26 (2009) 085002).

• An exact spherically symmetric static solution of the set of six MOG field equations is obtained, choosing suitable initial conditions for the unknown functions A, B, G, ω, μ and

$$\phi_t = -Q_5 \frac{e^{-\mu r}}{r},$$

• The metric is given by

$$ds^2 = Bdt^2 - Adr^2 - r^2 d\Omega^2,$$

where Q_5 is the fifth force charge proportional to mass M: $Q_5 = \kappa M$. This is possible in Maxwell-Proca theory for $\nabla^\mu J_\mu \neq 0$.

$$B(r) \sim 1 - \frac{2(1+\alpha)G_N M}{r} + \frac{(1+\alpha)G_N^2 M^2}{r^2}.$$

This expression for $B(r)$ is valid when r is at least several times the Schwarzschild radius.

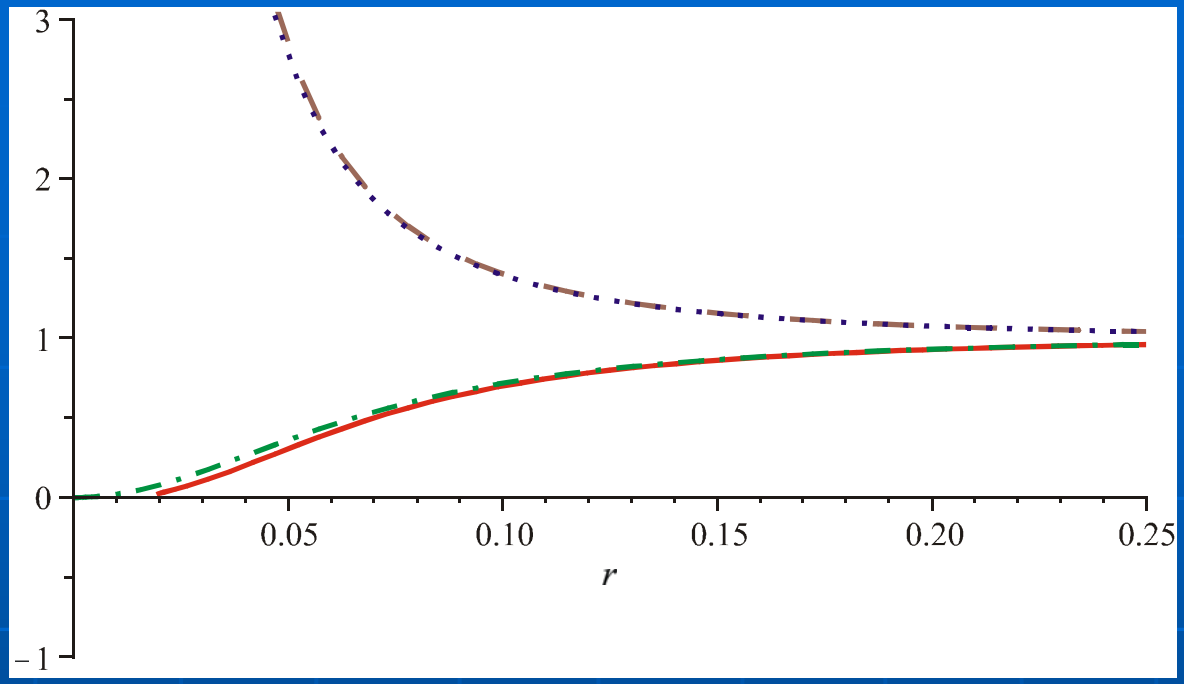

Comparing MOG numerical solutions to the Reissner-Nordström solution, for a $10^{11}\,M_{\odot}$ source mass. The MOG parameters A (solid red line) and B (dashed brown line) are plotted along with the Reissner-Nordström values of A (dash-dot green line) and B (dotted blue line). Horizontal axis is in pc. We observe that the A parameter reaches 0 at $r \sim 0.02$ pc. The Schwarzschild radius of a $10^{11}\,M_{\odot}$ mass is ~ 0.01 pc.

- The MOG vacuum solution, interior matter solutions for stars and stellar collapse are being analyzed. Significant modifications of the standard black hole GR solution are expected to be discovered.

- The equation of motion of a test particle is given by

$$m\left(\frac{du^\mu}{ds}+\Gamma^\mu_{\alpha\beta}u^\alpha u^\beta\right)=-\alpha\kappa\omega m B^\mu{}_\nu u^\nu.$$

- For weak fields the MOG acceleration law is

$$\frac{d^2r}{dt^2}=-\frac{G_N M}{r^2}\left[1+\alpha-\alpha(1+\mu r)e^{-\mu r}\right],$$

$$\alpha=\frac{M}{\left(\sqrt{M}+E\right)^2}\left(\frac{G_\infty}{G_N}-1\right),\qquad \mu=\frac{D}{\sqrt{M}},$$

$$D\cong 6250 M_\Theta^{1/2}\,\mathrm{kpc}^{-1},$$
$$E\cong 25000 M_\Theta^{1/2},$$
$$G_\infty\cong 20 G_N,$$

$$\frac{d^2r}{dt^2}=-\frac{G_{\rm eff}M}{r^2},\qquad G_{\rm eff}=G_N\left[1+\alpha-\alpha(1+\mu r)e^{-\mu r}\right].$$

- Making the assumption that $M=M(r)$ holds, the MOG Poisson equation is

$$\begin{aligned}\nabla^2\Phi &= 4\pi G_N\rho(\mathbf{r})+\mu^2\Phi_Y(\mathbf{r})\\ &= 4\pi G_N\rho(\mathbf{r})+\alpha\mu^2 G_N\int\frac{e^{-\mu|\mathbf{r}-\tilde{\mathbf{r}}|}}{|\mathbf{r}-\tilde{\mathbf{r}}|}\rho(\tilde{\mathbf{r}})\,d^3\tilde{\mathbf{r}}.\end{aligned}$$

3. Fitting Galaxy Rotation Curves and Clusters

• A fitting routine has been applied to fit a large number of galaxy rotation curves (101 galaxies), using photometric data (58 galaxies) and a core model (43 galaxies) (J. R. Brownstein and JWM, 2005; J. R. Brownstein, 2009). The fits to the data are remarkably good for STVG. For the photometric data, only one parameter, the mass-to-light ratio M/L, is used.

• A large sample of X-ray mass profile cluster data (106 clusters) has also been well fitted (J. R. Brownstein and JWM, 2005; JWM and V. T. Toth, 2007,2008; J. R. Brownstein, 2008).

• The rotational velocity curves become the Kepler-Newtonian curves at large distances from the galaxies (satellites).

•The Tully-Fisher law is satisfied by MOG: $v_c^2 \propto \frac{M}{\sqrt{M}} = \sqrt{M}$.

• For every feature in the surface brightness distribution, MOG produces a corresponding feature in the predicted rotation curve (matching the observed rotation curve).

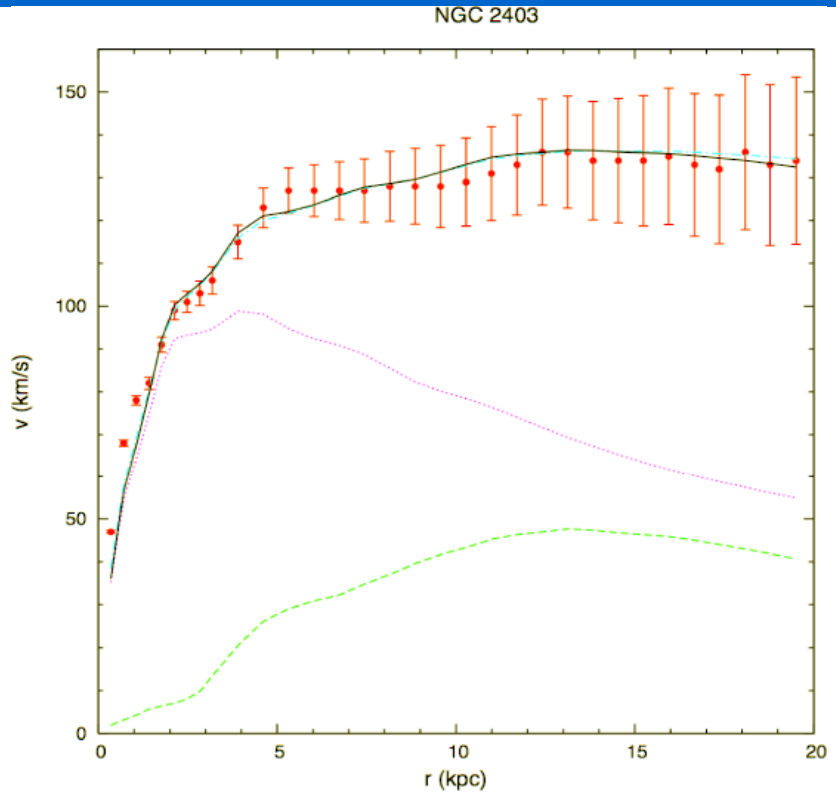

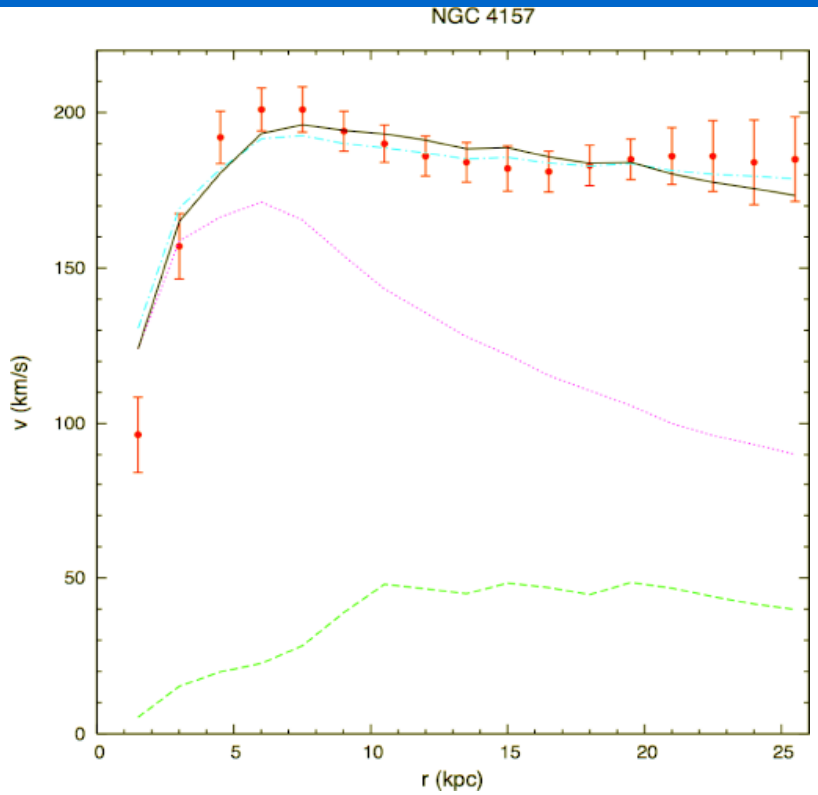

Photometric fits to galaxy rotation curves. There are 4 benchmark galaxies presented here; each is a best fit via the single parameter $(M/L)_{stars}$ based on the photometric data of the gaseous (HI plus He) and luminous stellar disks. The radial coordinate (horizontal axis) is given in kpc and the rotational velocity (vertical axis) in km/s. The red points with error bars are the observations, the solid black line is the rotation curve determined from MOG, and the dash-dotted cyan line is the rotation curve determined from MOND. The other curves are the Newtonian rotation curves of the various separate components: the long-dashed green line is the rotation curve of the gaseous disk (HI plus He) and the dotted magenta curve is that of the luminous stellar disk.

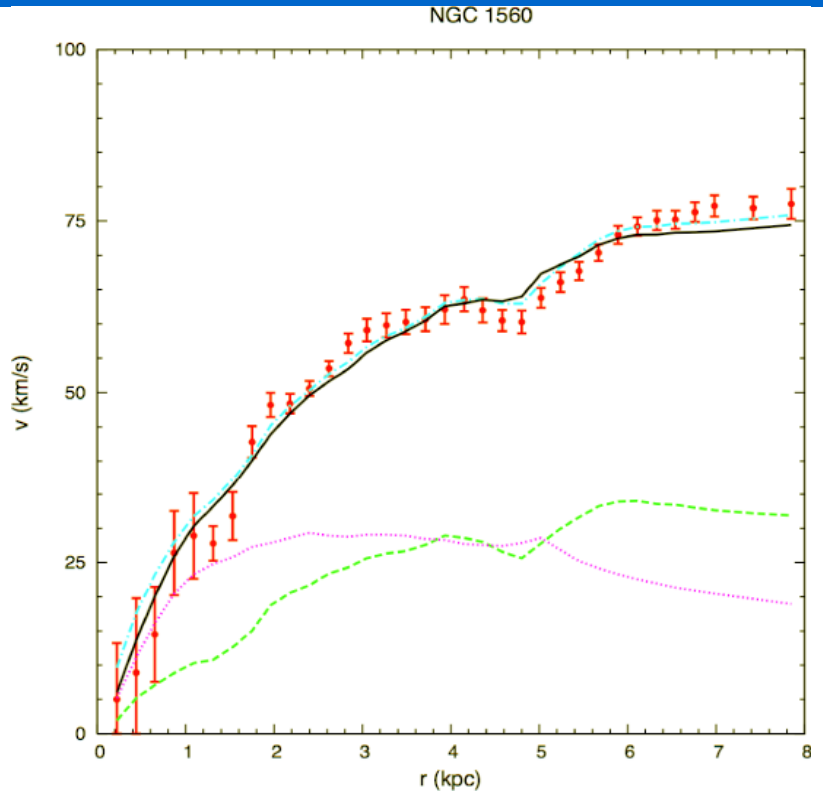

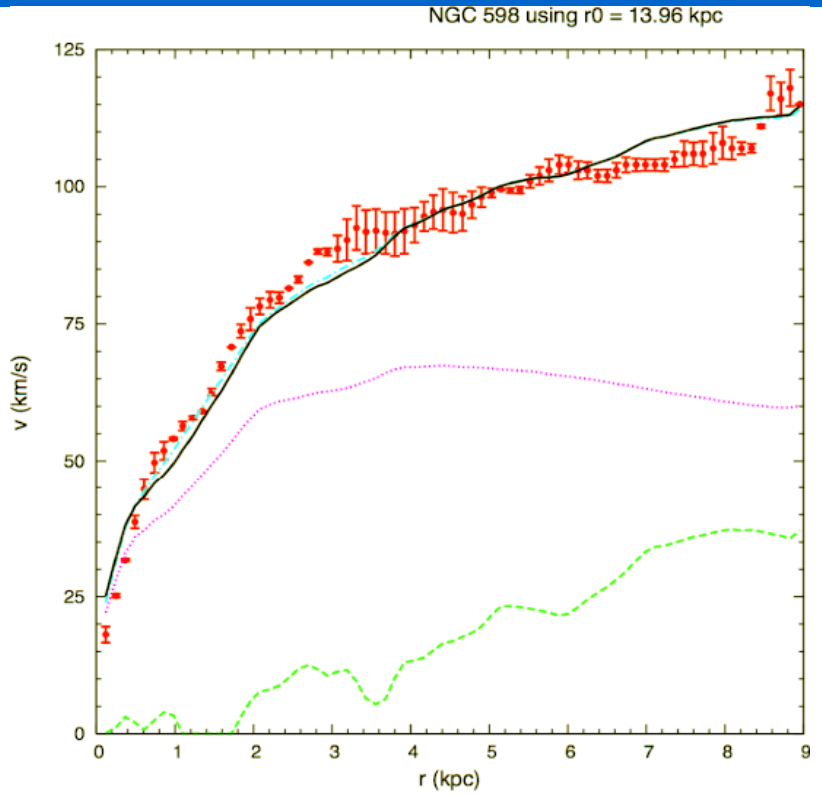

Photometric fits to galaxy rotation curves. There are 4 benchmark galaxies presented here; each is a best fit via the single parameter $(M/L)_{stars}$ based on the photometric data of the gaseous (HI plus He) and luminous stellar disks. The radial coordinate (horizontal axis) is given in kpc and the rotational velocity (vertical axis) in km/s. The red points with error bars are the observations, the solid black line is the rotation curve determined from MOG, and the dash-dotted cyan line is the rotation curve determined from MOND. The other curves are the Newtonian rotation curves of the various separate components: the long-dashed green line is the rotation curve of the gaseous disk (HI plus He) and the dotted magenta curve is that of the luminous stellar disk.

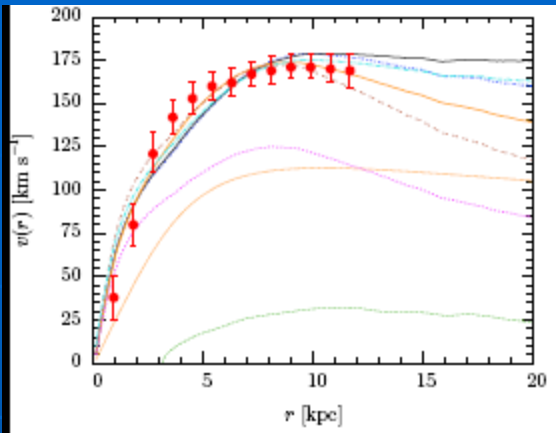

HSB (a) NGC 3877

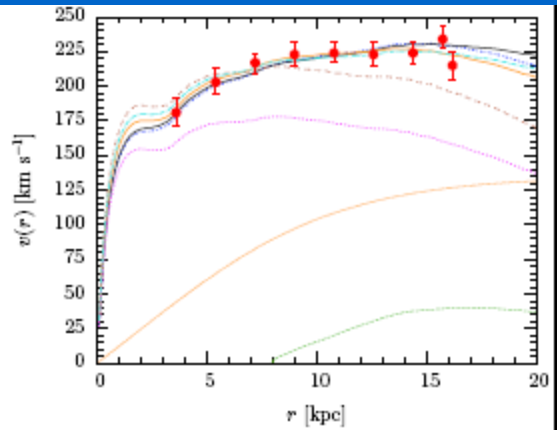

HSB (b) NGC 3953

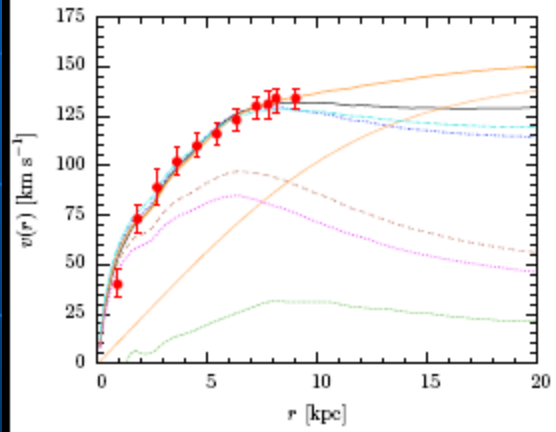

HSB (c) NGC 3972

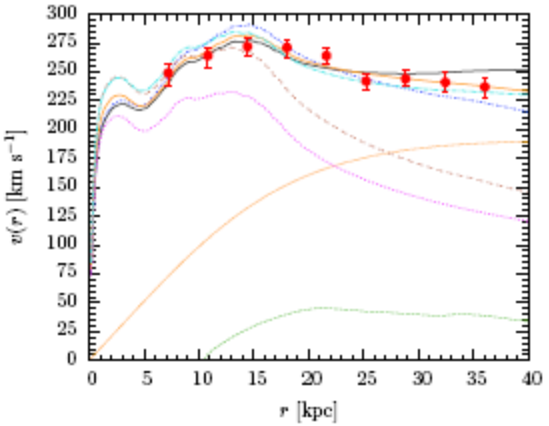

HSB (d) NGC 3992

J. R. Brownstein's doctoral thesis

$v(r)$	red filled circles with error bars
Component	**with lines**
Actual HI gas	green dashed line
Stellar disk [$\Upsilon = 1$]	magenta dotted line
Dark matter halo	orange fine-dotted line

Theory	**with lines**
Newtonian core	brown dot-dotted line
STVG	black solid line
MSTG	blue short dash-dotted line
MOND	cyan long dash-dotted line
Dark matter	orange solid line

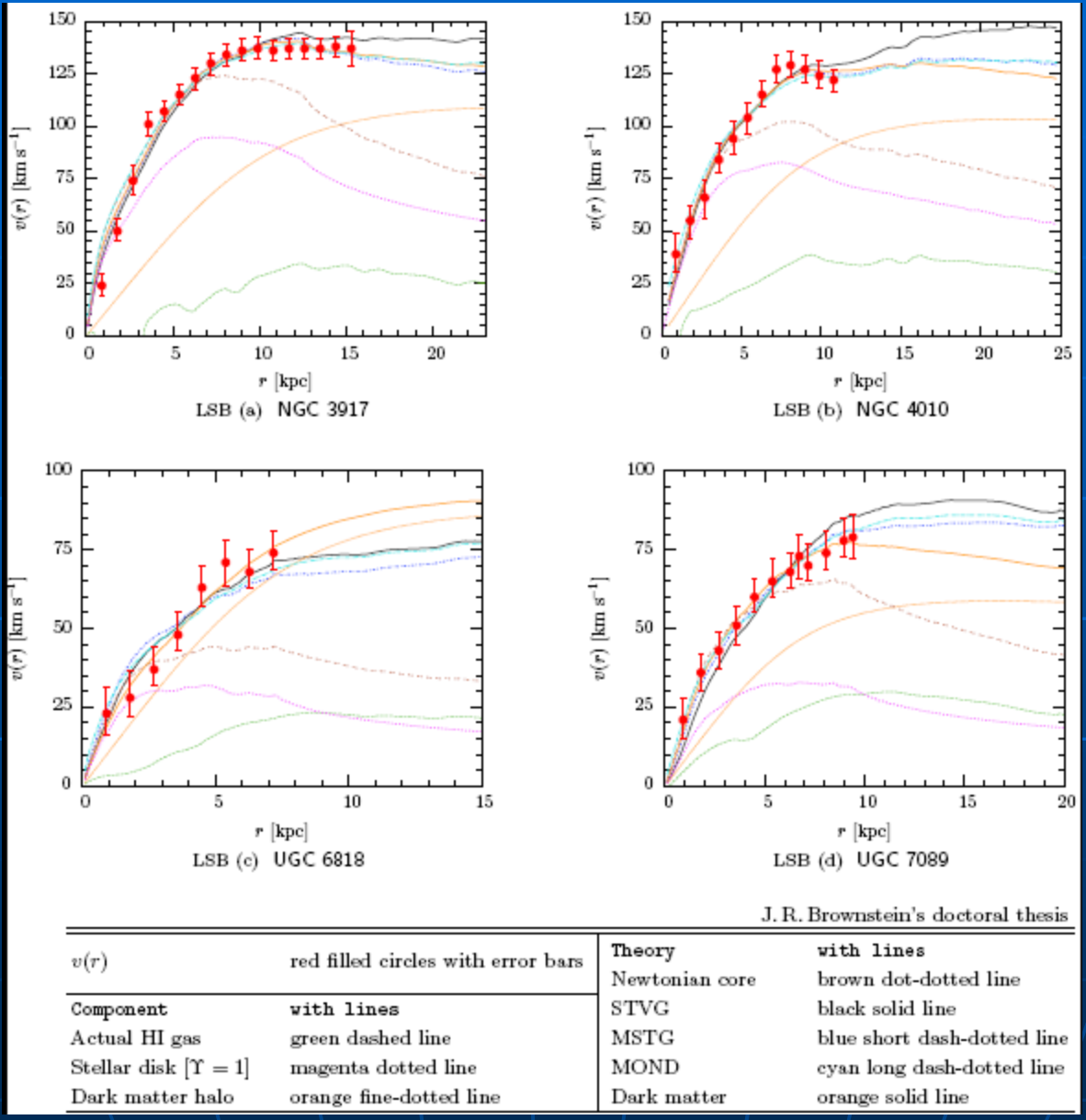

J. R. Brownstein's doctoral thesis

$v(r)$	red filled circles with error bars
Component	**with lines**
Actual HI gas	green dashed line
Stellar disk [$\Upsilon = 1$]	magenta dotted line
Dark matter halo	orange fine-dotted line

Theory	**with lines**
Newtonian core	brown dot-dotted line
STVG	black solid line
MSTG	blue short dash-dotted line
MOND	cyan long dash-dotted line
Dark matter	orange solid line

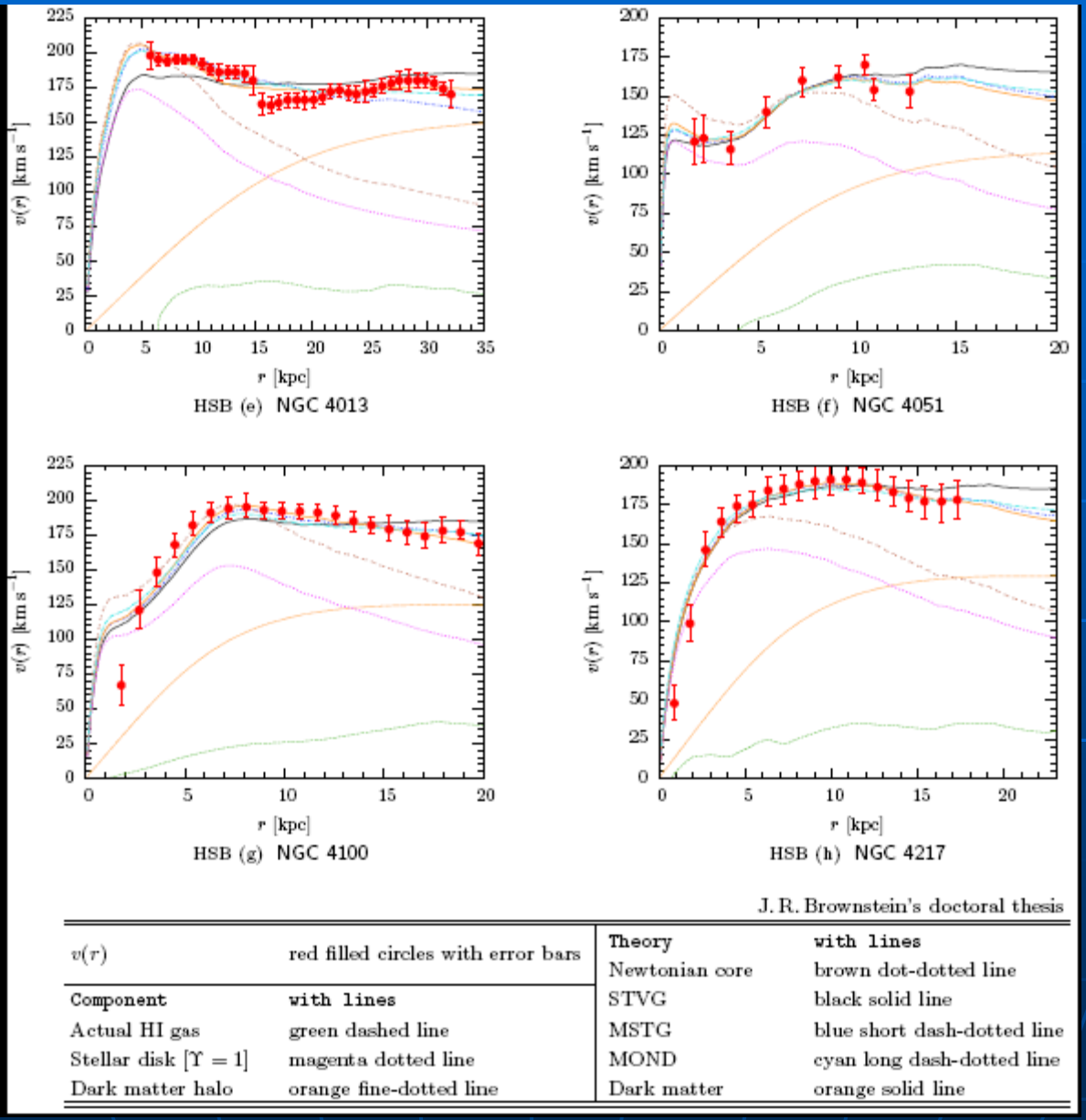

J. R. Brownstein's doctoral thesis

$v(r)$	red filled circles with error bars
Component	**with lines**
Actual HI gas	green dashed line
Stellar disk [$\Upsilon = 1$]	magenta dotted line
Dark matter halo	orange fine-dotted line

Theory	**with lines**
Newtonian core	brown dot-dotted line
STVG	black solid line
MSTG	blue short dash-dotted line
MOND	cyan long dash-dotted line
Dark matter	orange solid line

- MOG predictions for mass profiles in clusters.

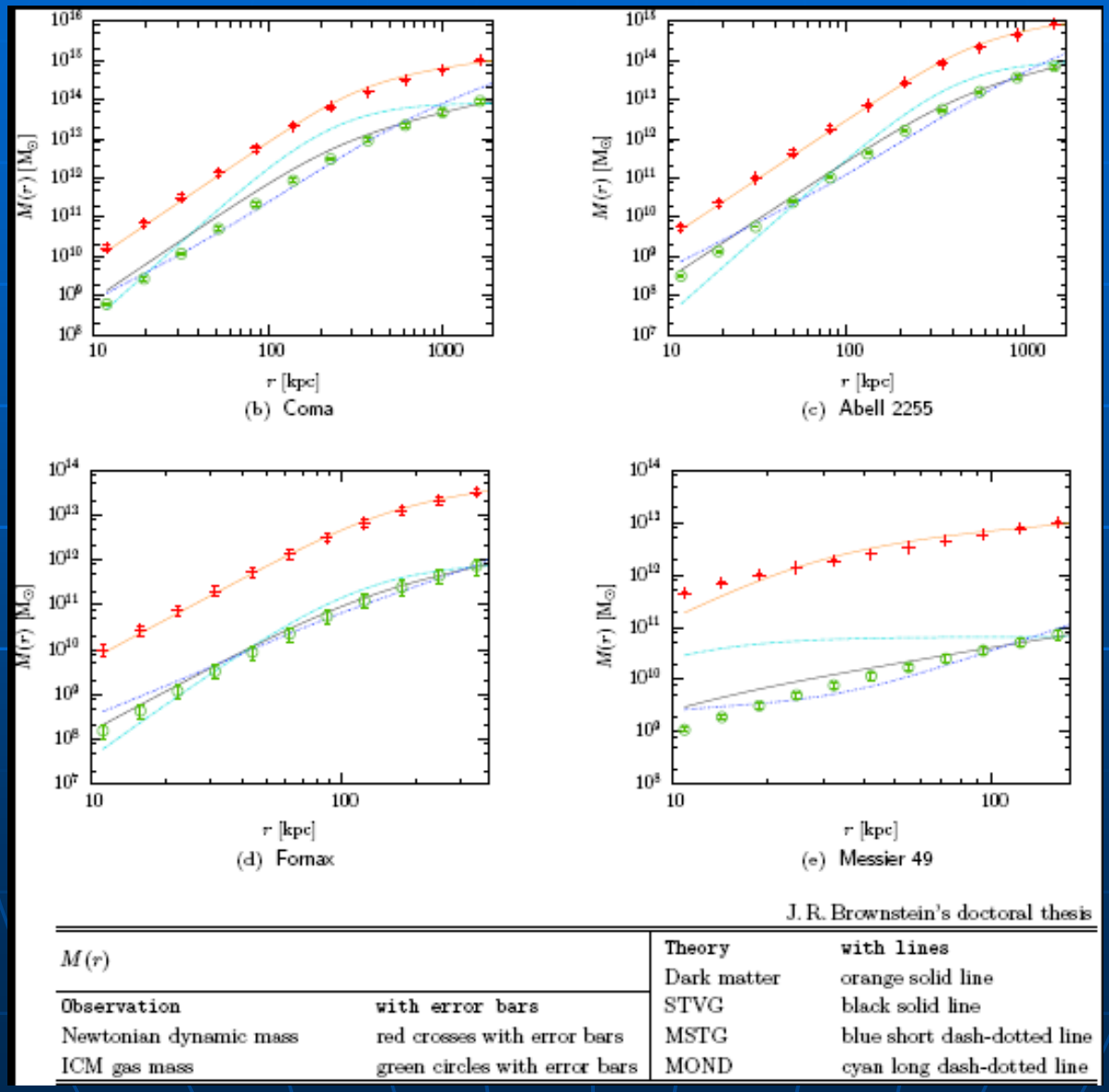

J. R. Brownstein's doctoral thesis

$M(r)$		Theory	with lines
Observation	with error bars	Dark matter	orange solid line
Newtonian dynamic mass	red crosses with error bars	STVG	black solid line
ICM gas mass	green circles with error bars	MSTG	blue short dash-dotted line
		MOND	cyan long dash-dotted line

• The merging clusters 1E0657-56 ($z = 0.296$) (discovered by Tucker et al. 1995) is claimed to prove empirically the existence of dark matter (Clowe et al. 2003-2006, Bradac et al. 2006). Due to the collision of two clusters, the dissipationless stellar component and the X-ray emitting plasma are spatially segregated. The claim is that the gravitationally lensing maps show that the gravitational potential does not trace the plasma distribution – the dominant baryonic mass component – but rather approximately traces the distribution of galaxies.

• *MOG explains the 8σ significance spatial offset of the center of the total mass from the center of the baryonic mass peaks (J. R. Brownstein and JWM, MNRAS 2006).*

The bullet cluster 1E0657-56

The “anti-bullet” cluster Abell 520

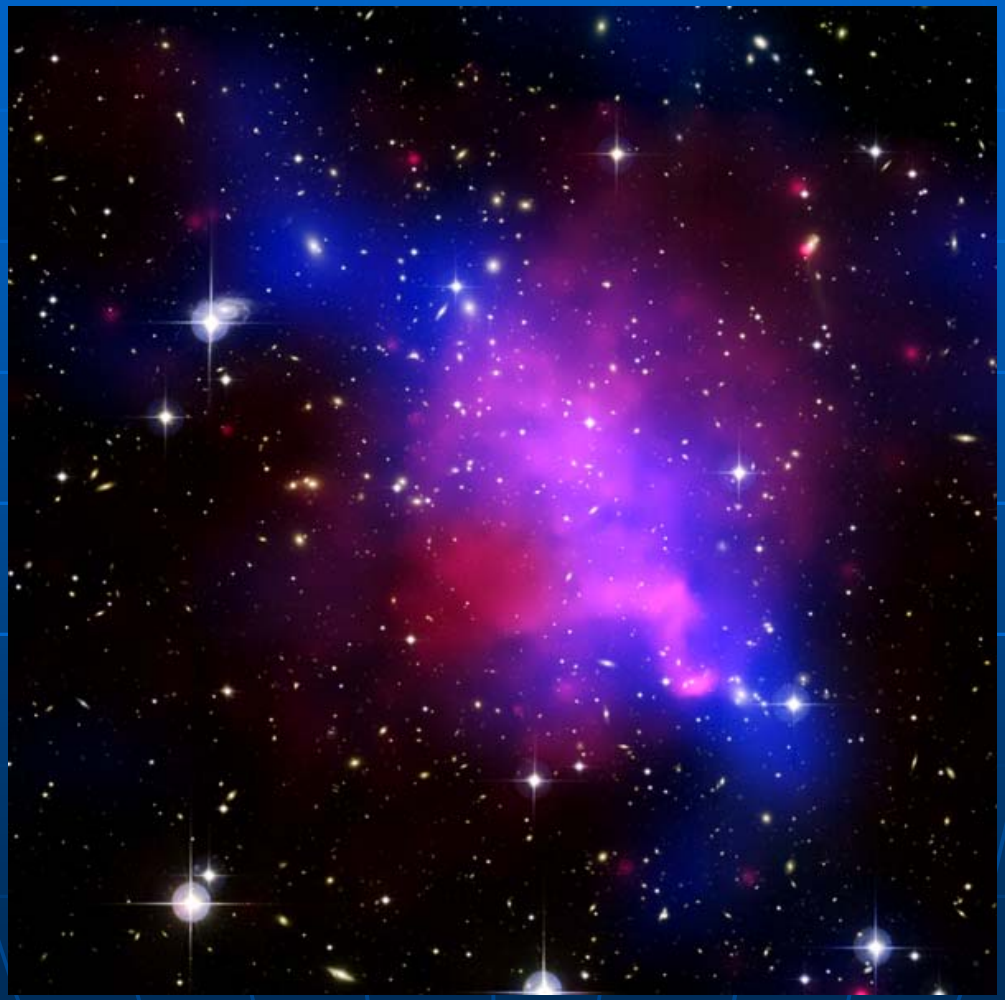

Predictions for globular clusters

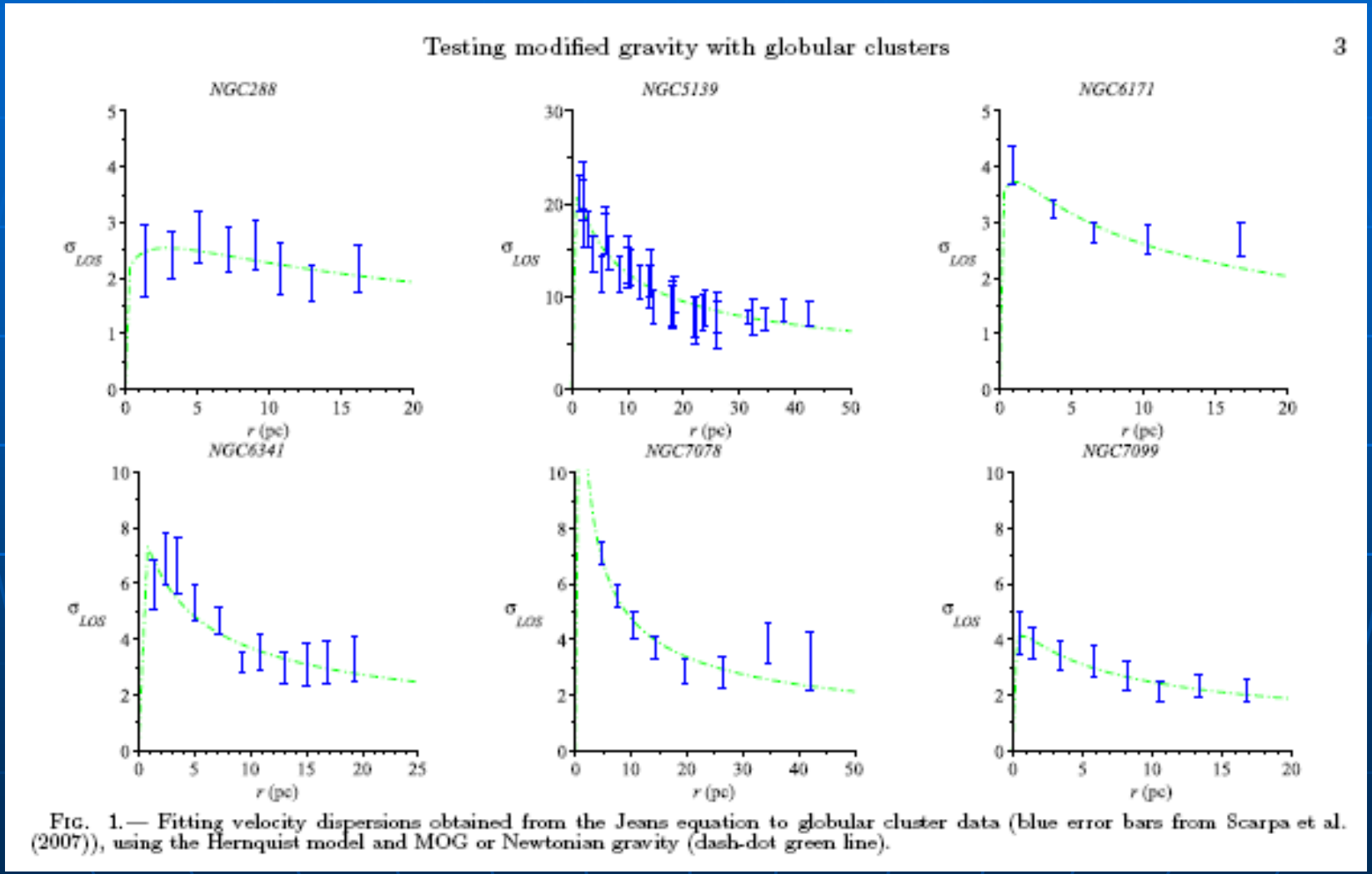

FIG. 1.— Fitting velocity dispersions obtained from the Jeans equation to globular cluster data (blue error bars from Scarpa et al. (2007)), using the Hernquist model and MOG or Newtonian gravity (dash-dot green line).

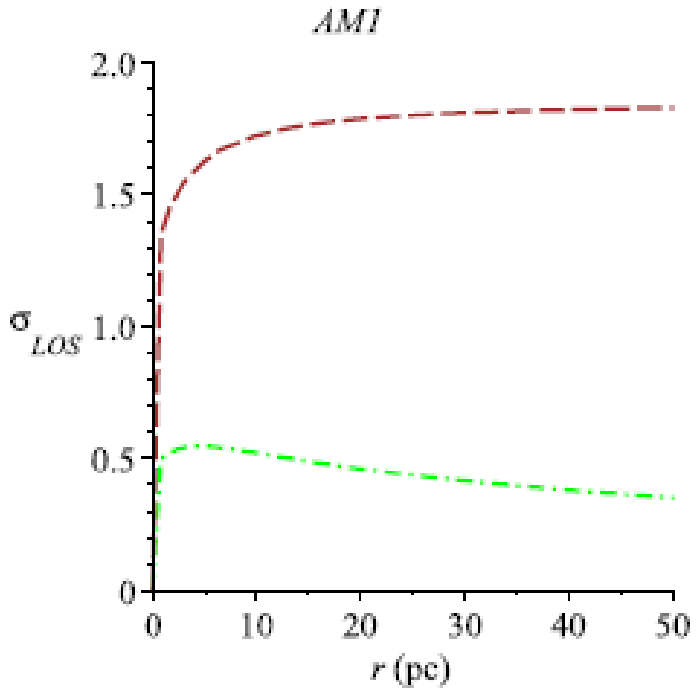

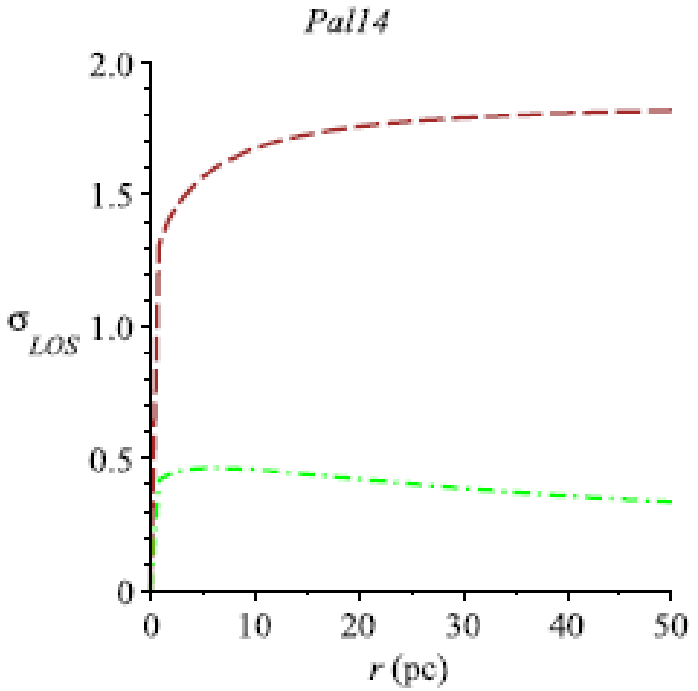

FIG. 2.— Predicted velocity dispersion curves for two distant GCs. Dash-dot line (green) is the prediction obtained using MOG or Newtonian gravity; dashed (brown) curve is the MOND prediction. In both cases, we used $M/L = 2$ and we equated the parameter r_0 of the Hernquist model with the half-light radius.

$$M/L = (2.2 \pm 0.4)\ M_\odot/L_\odot.$$

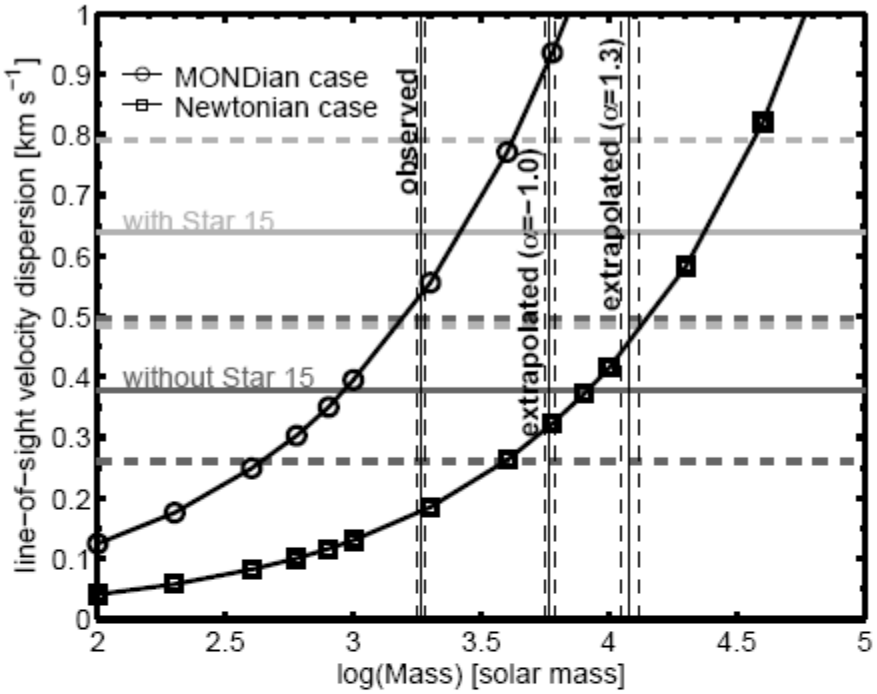

Fig. 10.— Theoretically predicted velocity dispersion as a function of mass. The two black curves are the predictions in MONDian dynamics (open circles) and in classical Newtonian dynamics (open squares). The observed velocity dispersions (and the errors) are drawn as the two horizontal lines, the light gray without Star 15, dark gray with Star 15. The vertical lines mark the observed lower mass limit and the two extrapolated lower mass limits.

K. Jordi1, E. K. Grebel, M. Hilker, H. Baumgardt, M. Frank, P. Kroupa, H. Haghi, P. Cˆot´e, and S. G. Djorgovski.

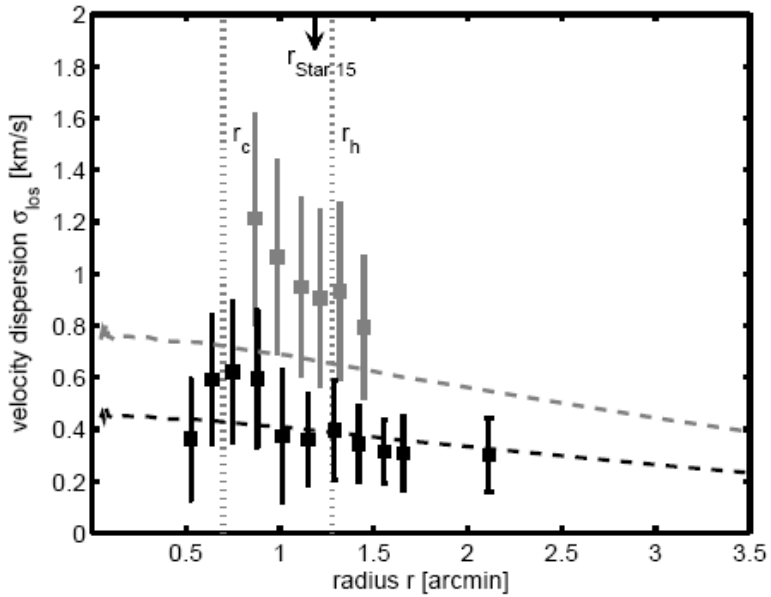

Fig. 11.— The velocity dispersion profile of Pal 14 using running bins with six stars in each bin. The black squares denote the velocity dispersion without Star 15. The gray squares denote these bins where Star 15 was included. The black and gray dashed curves are the theoretical dispersion profiles if Star 15 was included and excluded, respectively. The vertical, dotted lines are the core and half-light radii (H06), respectively. The arrow at the top of the plot marks the radial distance of Star 15 from the cluster center.

4. MOG Cosmology

- We adopt a FLRW background spacetime:

$$ds^2 = dt^2 - a^2(t)\left(\frac{dr^2}{1-kr^2} + r^2 d\Omega^2\right), \qquad \phi_0 \equiv \phi \neq 0, \qquad \phi_i = 0, \text{ and } B_{\mu\nu} = 0.$$

- The modified Friedmann equations are (JWM & V. T. Toth, 2008):

$$H^2 + \frac{k}{a^2} = \frac{8\pi G\rho}{3} - \frac{4\pi}{3}\left(\frac{\dot{G}^2}{G^2} + \frac{\dot{\mu}^2}{\mu^2} - \dot{\omega}^2 - G\omega\mu^2\phi_0^2\right) + \frac{8\pi}{3}\left(\omega G V_\phi + \frac{V_G}{G^2} + \frac{V_\mu}{\mu^2} + V_\omega\right) + \frac{\Lambda}{3} + H\frac{\dot{G}}{G},$$

$$\frac{1}{a}\frac{d^2a}{dt^2} = -\frac{4\pi G}{3}(\rho + 3p) + \frac{8\pi}{3}\left(\frac{\dot{G}^2}{G^2} + \frac{\dot{\mu}^2}{\mu^2} - \dot{\omega}^2 - G\omega\mu^2\phi_0^2\right) + \frac{8\pi}{3}\left(\omega G V_\phi + \frac{V_G}{G^2} + \frac{V_\mu}{\mu^2} + V_\omega\right) + \frac{\Lambda}{3} + H\frac{\dot{G}}{2G} + \frac{1}{2G}\frac{d^2G}{dt^2} - \frac{\dot{G}^2}{G^2},$$

$$\frac{d^2G}{dt^2} + 3H\dot{G} - \frac{3}{2}\frac{\dot{G}^2}{G} + \frac{G}{2}\left(\frac{\dot{\mu}^2}{\mu^2} - \dot{\omega}^2\right) + \frac{3}{G}V_G - V_G' + G\left(\frac{V_\mu}{\mu^2} + V_\omega\right) + \frac{G}{8\pi}\Lambda - \frac{3G}{8\pi}\left(\frac{1}{a}\frac{d^2a}{dt^2} + H^2\right) = 0,$$

$$\frac{d^2\omega}{dt^2} + 3H\dot{\omega} - \frac{\dot{G}}{G}\dot{\omega} - \frac{1}{2}G\mu^2\phi_0^2 + GV_\phi + V_\omega' = 0, \qquad \frac{d^2\mu}{dt^2} + 3H\dot{\mu} - \frac{\dot{\mu}^2}{\mu} - \frac{\dot{G}}{G}\dot{\mu} + G\omega\mu^3\phi_0^2 + \frac{2}{\mu}V_\mu - V_\mu' = 0.$$

• The MOG cosmology equations possess an exact numerical solution, given initial conditions.

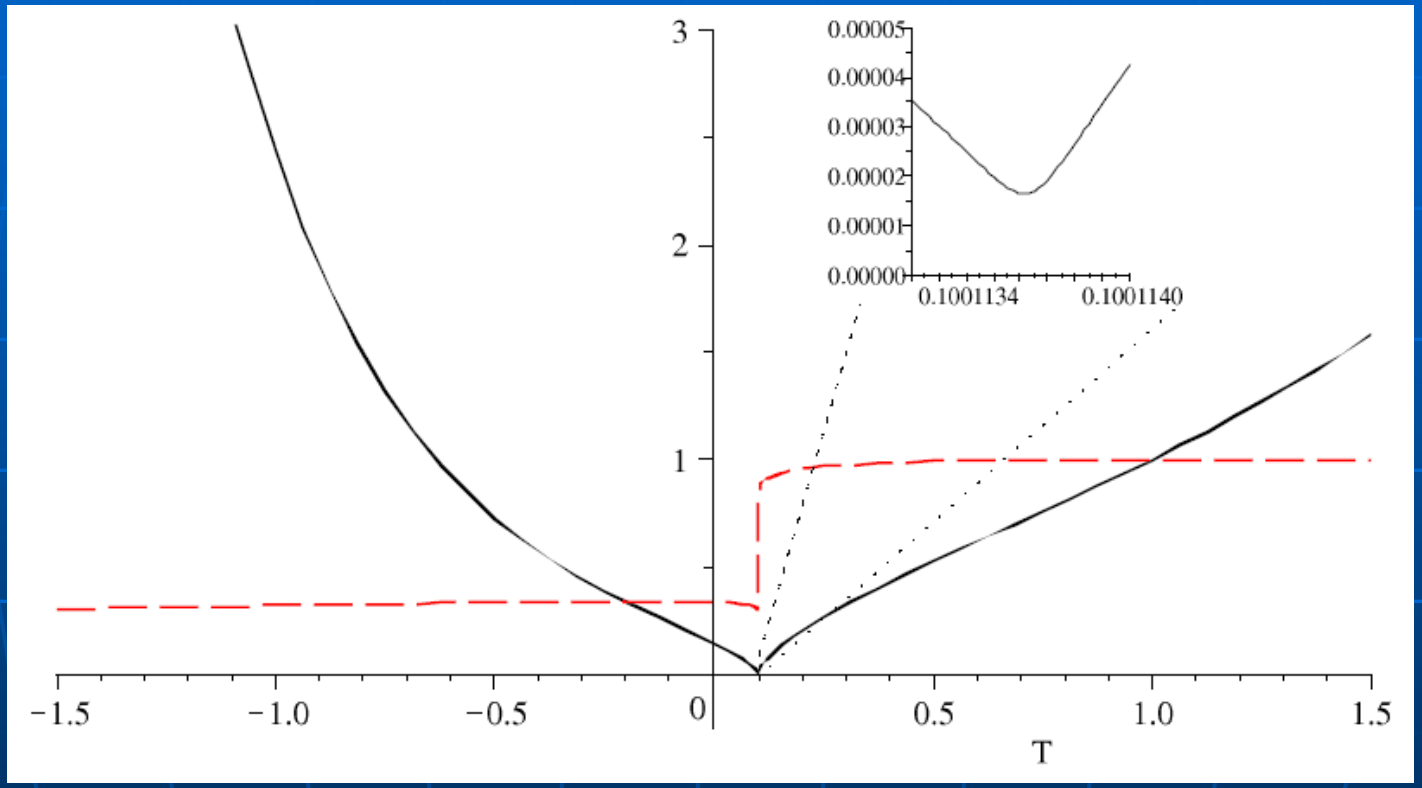

The MOG "bouncing" cosmology. The horizontal axis represents time, measured in Hubble units of H_0^{-1}. The solid (black) line is a/a_0, the scale factor normalized to the present epoch. The dashed (red) line is G/G_0. The inset shows details of the bounce, demonstrating that a smooth bounce occurs even as the matter density of the universe is more than 10^{14} times its present value.

• The correlation function for the temperature differences across the sky for a given angle θ takes the form:

$$C(\theta)=\frac{1}{4\pi}\sum_{l=2}^{\infty}(2l+1)C_l P_l\cos\theta,$$

• We use a modified form of the analytic calculation of C_l given by Mukhanov (2006) to obtain a fit to the acoustical peaks in the CMB for $100 < l < 1200$. Assuming that the baryon fluid dominates, the adopted density parameters are

$$\Omega_{bN}=\frac{8\pi G_N\rho_b}{3H^2}\sim 0.04, \qquad \Omega_m=\Omega_{b\mathrm{eff}}=\frac{8\pi G_{\mathrm{eff}}\rho_b}{3H^2}\sim 0.3, \qquad \Omega_G=\frac{\Lambda_G}{H^2}\sim 0.7,$$

$$\xi=\frac{1}{3c_s^2}-1=\frac{3}{4}\left(\frac{\rho_b}{\rho_\gamma}\right)\sim 0.6, \qquad r_h\sim 0.03, \qquad r_p\sim 0.01, \qquad l_f\sim 1580, \qquad l_s\sim 1100.$$

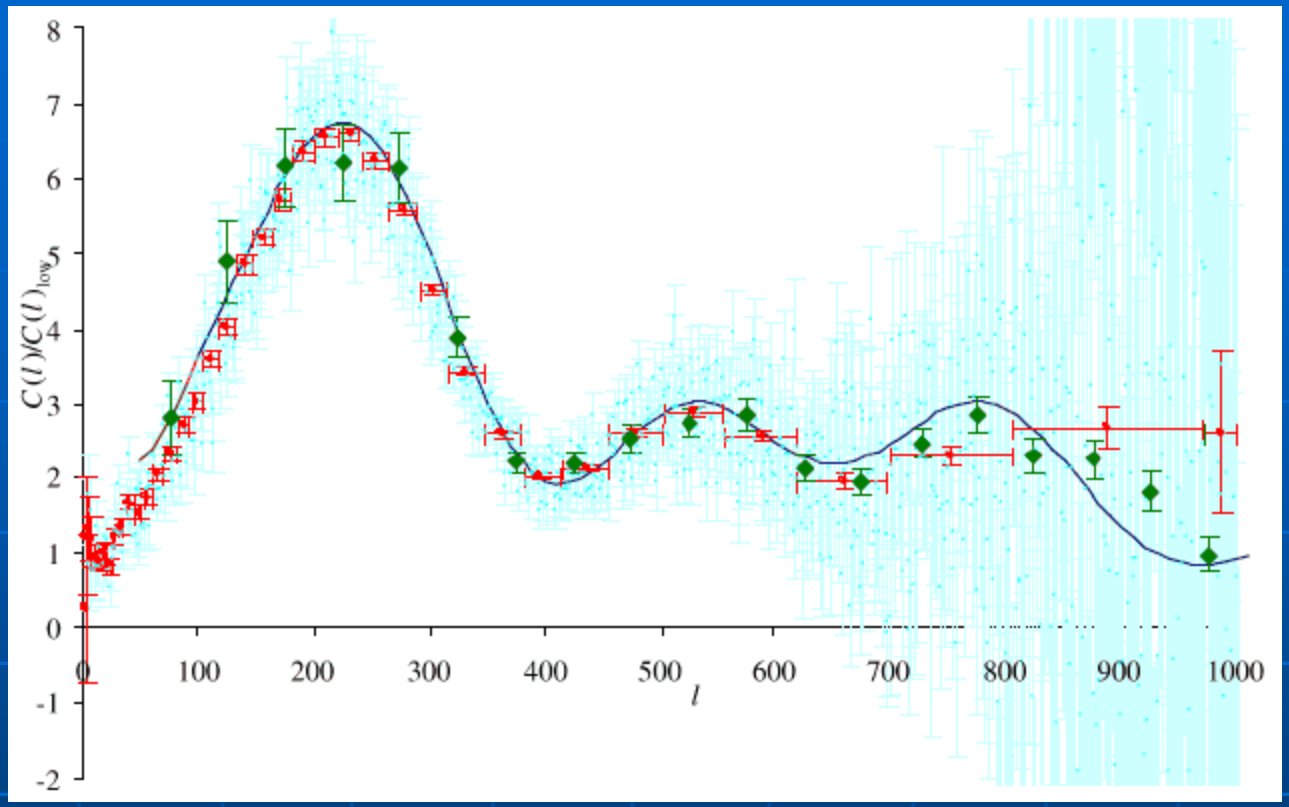

MOG and the acoustic power spectrum. Calculated using $\Omega_M = 0.3$, Ω_b=0.035, $H_0 = 71$ km/s/Mpc. Also shown are the raw WMAP 3-year data set (light blue), binned averages with horizontal and vertical error bars provided by the WMAP project (red), and data from the Boomerang experiment (green).

• The role played by CDM in the standard ΛCDM model is replaced in MOG by the significant deepening of the gravitational wells before recombination with $G_{\text{eff}} \sim 7G_N$, which traps the baryons. This reduces the baryon dissipation due to the photon coupling pressure (Silk damping) and the third and higher peaks in the acoustical oscillation spectrum are not suppressed due to finite thickness and baryon drag effects. The effective baryon density $\Omega_{b\text{eff}} = (1+Z)\Omega_{bN} \sim 7\Omega_{bN} \sim 0.3$ dominates before recombination and we fit the acoustical spectrum without a collisionless dark matter component.

• The decelerating parameter q can be expressed from the MOG Friedmann equations as

$$q = \frac{1}{2}(1+3w_{\text{eff}})\left(1+\frac{k}{\dot{a}^2}\right) - \frac{1}{2}(1+w_{\text{eff}})\frac{\Lambda}{H^2}, \quad \Omega_m = \frac{8\pi G_{\text{eff}}\rho_m}{3H^2}, \quad \Omega_G = \frac{\Lambda_G}{H^2}, \quad \Omega_m + \Omega_G = 1, \quad \dot{\Lambda}_G \sim 0.$$

• The effective MOG equation of state is $w_{\text{eff}} < 0$ and descends below $-1/3$ when the universe is about 2/3 its present age. This allows q to be negative, resulting in an accelerating universe even though $\Lambda = 0$.

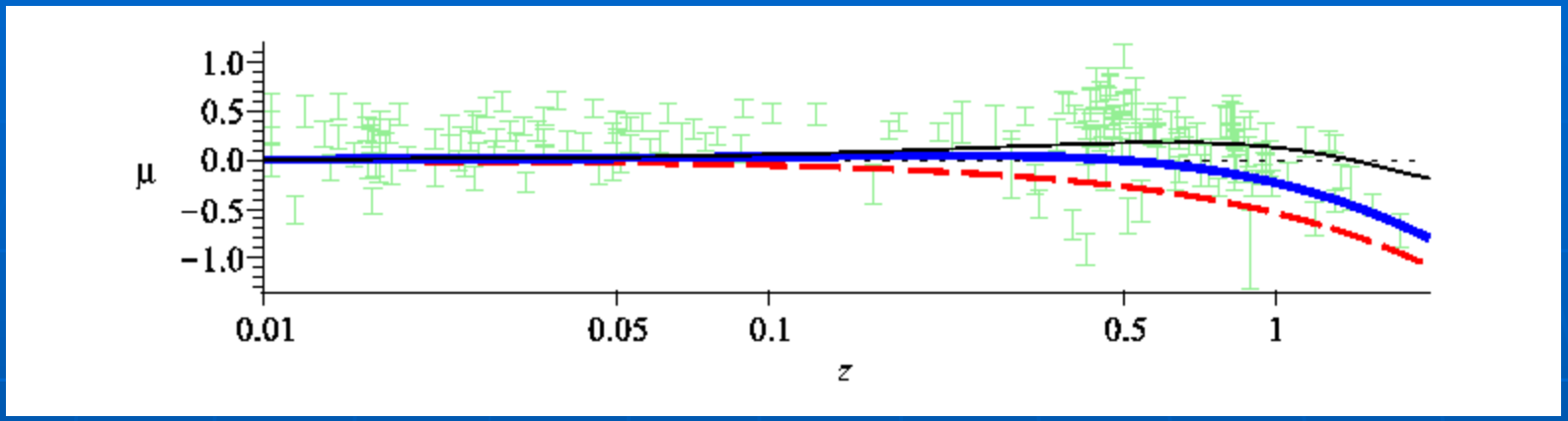

Type Ia supernova luminosity-redshift data and the MOG/ΛCDM predictions. No astrophysical dimming was applied. The horizontal axis corresponds to the $q = 0$ empty universe. The MOG result is represented by a thick (blue) line. Dashed (red) line is a matter-dominated Einstein de-Sitter universe with $\Omega_M = 1$, $q = 0.5$. Thin (black) line is the ΛCDM prediction.

• The gravitational instability governing over-densities $\delta = \delta\rho/\rho$ reads schematically:

$$\frac{\partial^2 \delta}{\partial t^2} + [\text{Pressure} - \text{Gravity}]\delta = 0.$$

• If pressure is low δ grows exponentially, while if pressure is high δ oscillates with time. The effective increase in the gravitational constant $G_{\text{eff}} \sim 7G_N$ produces growth at earlier times before recombination copying the effects of cold dark matter. Thus, the observed power spectrum can be predicted by MOG without cold dark matter.

• A generic test to distinguish between CDM and MOG is to observe unit oscillations in the matter power spectrum, produced by baryons. The finite size of samples and the associated window functions are masking any such oscillations in the power spectrum data. These oscillations may become observable as the galaxy surveys increase in size and the window functions narrow in size.

5. MOG Verifiable Predictions

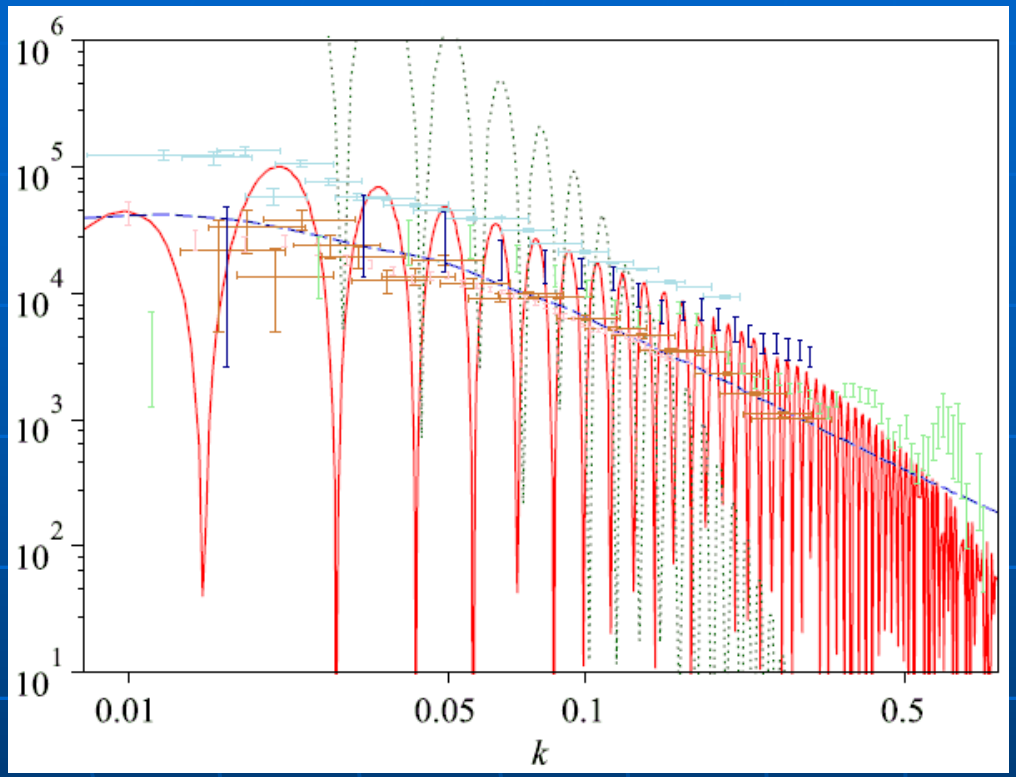

The matter power spectrum. Three models are compared against five data sets (see text): ΛCDM (dashed blue line, $\Omega_b = 0.035$, $\Omega_c = 0.245$, $\Omega_\Lambda = 0.72$, $H = 71$ km/s/Mpc), a baryon-only model (dotted green line, $\Omega_b = 0.035$, $H = 71$ km/s/Mpc), and MOG (solid red line, $\alpha = 19$, $\mu = 5h$ Mpc^{-1}, $\Omega_b = 0.035$, $H = 71$ km/s/Mpc.) Data points are colored light blue (SDSS 2006), gold (SDSS 2004), pink (2dF), light green (UKST), and dark blue (CfA).

$$T(k) = \frac{\Omega_b}{\Omega_m} T_b(k) + \frac{\Omega_c}{\Omega_m} T_c(k),$$

$$P(k) = T^2(k) P_0(k),$$

$$\frac{d^2\delta_{\mathbf{k}}}{dt^2} + 2H\dot{\delta}_{\mathbf{k}} + \left(\frac{c_s^2 k^2}{a^2} - 4\pi G_{\text{eff}} \rho \right) \delta_{\mathbf{k}} = 0,$$

$$G_{\text{eff}} = G_N \left\{ 1 + \alpha \left[1 - \left(1 + \frac{\mu a}{k} \right) e^{-\mu a/k} \right] \right\}.$$

• Verifiable prediction of matter power spectrum that distinguishes cold dark matter from MOG without exotic dark matter.

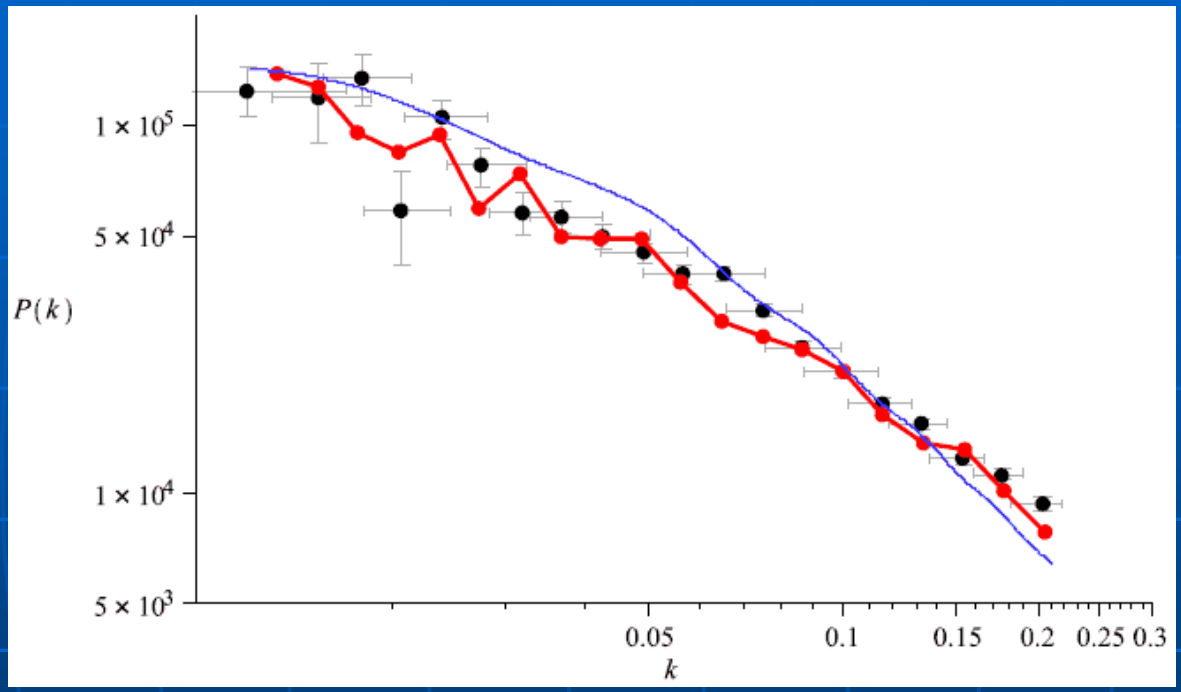

The effect of window functions on the power spectrum is demonstrated by applying the SDSS luminous red galaxy survey window functions to the MOG prediction. Baryonic oscillations are greatly dampened in the resulting curve (solid red line), yielding excellent agreement with the data after normalization. A normalized linear ΛCDM estimate is also shown (thin blue line) for comparison.

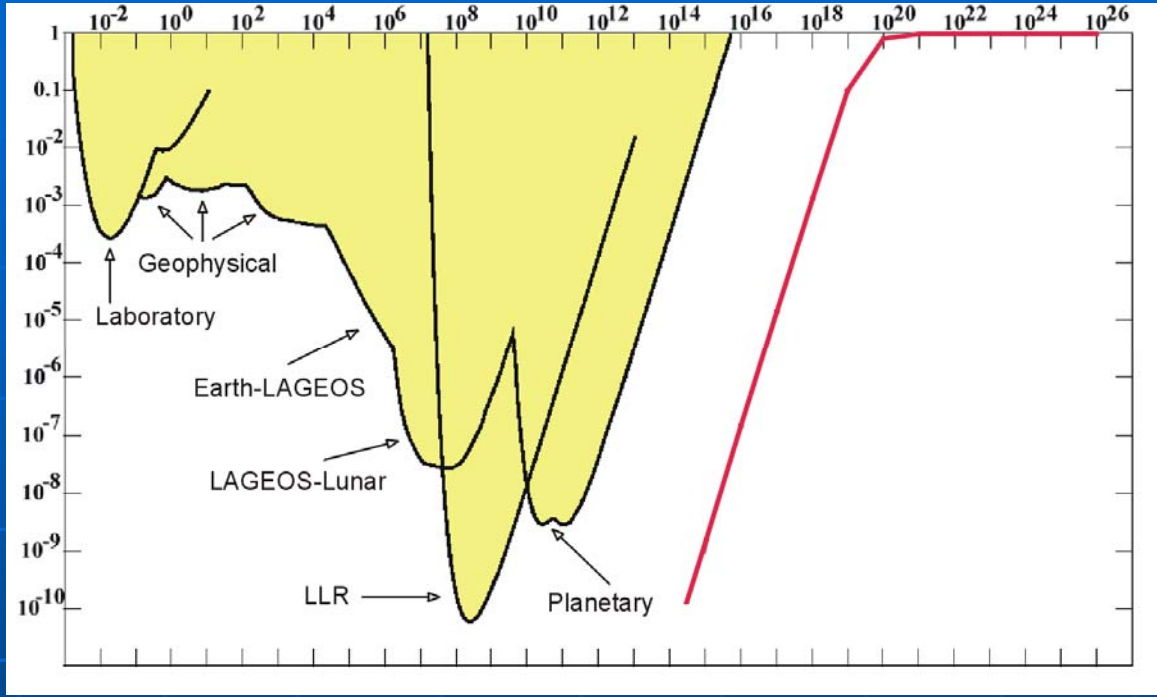

Predictions of the Yukawa-parameters from the MOG field equations are not in violation of solar system and laboratory constraints. Predicted values of λ (horizontal axis, in m) vs. α_Y are indicated by the solid red line. Plot adapted from Adelberger (2003).

$$|\alpha_Y| \sim 9 \times 10^{-14}.$$

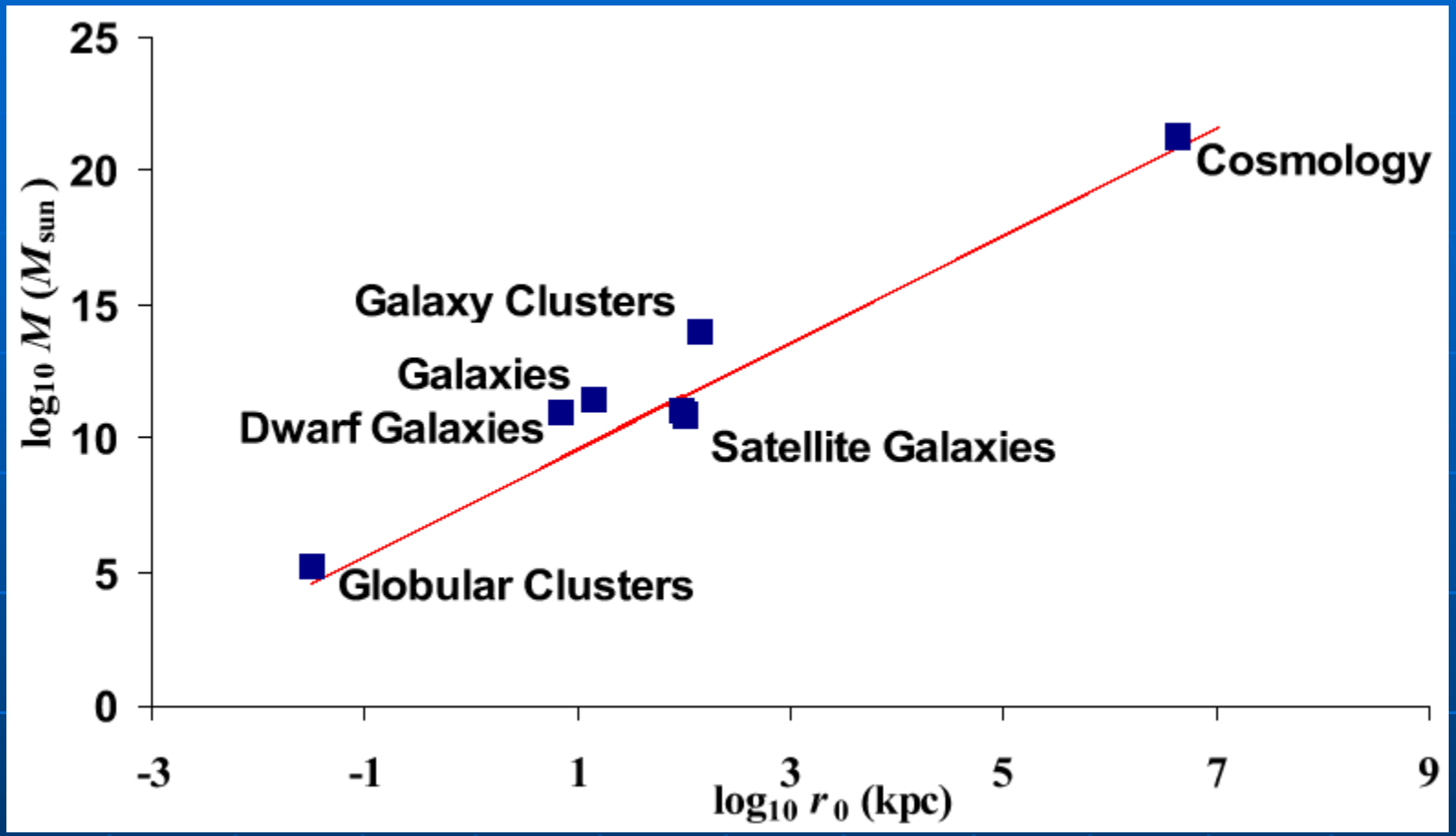

The relationship $\mu^2 M = \text{const.}$ between mass M and the Yukawa-parameter $r_0 = \mu^{-1}$ across many orders of magnitude remains valid. The solid red line represents our theoretical prediction.

• MOG does not satisfy Birkhoff's theorem. It can realize Mach's principle and explain the origin of inertia (JWM & V. T. Toth, 2009, Mon. Not. Roy. Astr. Soc. 395 (2009) L25). The inertial force arises as the influence of distant matter in the universe.

$$F = mg \qquad F_I = F(g),$$
$$F(g) \sim -mg, \qquad F_I + F(g) = 0.$$

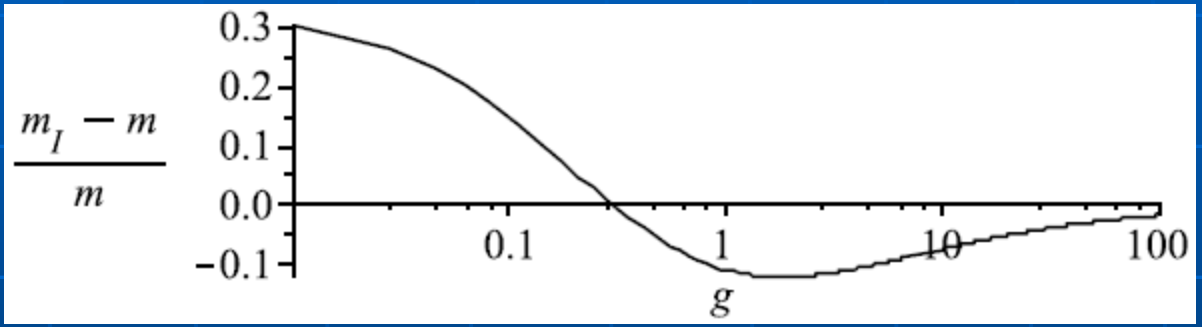

Does MOG violate the weak equivalence principle for very small accelerations? The horizontal axis in this plot is acceleration, measured in units of the "cosmic acceleration" $cH_0 \sim 7 \times 10^{-10}$ m/s^2. The vertical axis shows the predicted difference between inertial mass $m_I = -F(g)/g$ and passive gravitational mass m.

• Observational test in space of violation of equivalence principle at very small accelerations:

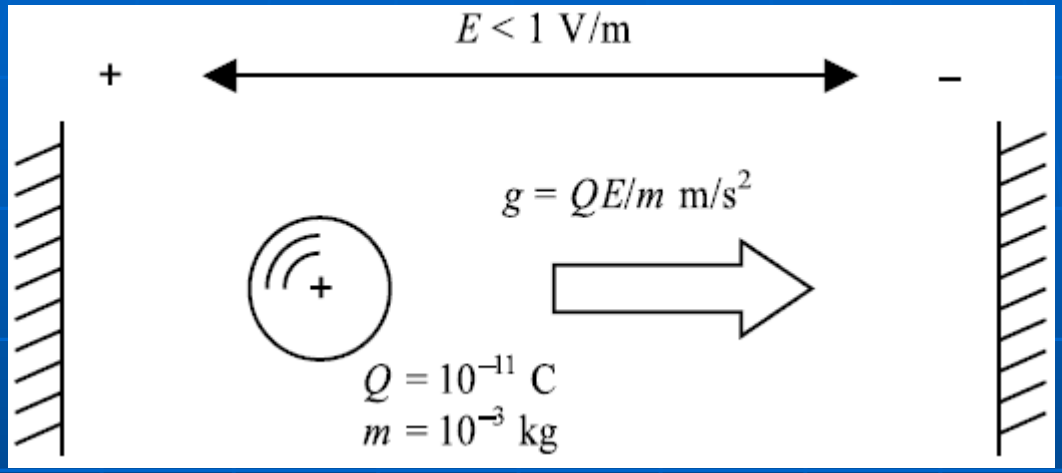

Schematic of a simple experiment that can be used to verify the validity of the force law $F = mg$ for very small accelerations. With the values presented here, a measurement of a deflection of ~1.8 mm over the course of ten minutes with an accuracy better than 10% is required, in order to measure the deficit in inertial mass. A smaller acceleration (corresponding to $E \sim 0.01$ V/m) could be used to measure an excess in inertial mass of up to ~30%.

6. Conclusions

• A stable and self-consistent modified gravity (MOG) is constructed from a pseudo-Riemannian geometry and a massive skew field obtained from the curl of a massive vector field (phion field) (STVG). The field equations are derived from a fully relativistic action principle. The static spherically symmetric solution of the field equations yields a modified Newtonian acceleration law with a distance scale dependence. The gravitational "constant" G, the effective mass and the coupling strength of the skew field run with distance scale r.

• A fit to galaxy rotations curves is obtained with only M/L as a free parameter without exotic dark matter. The mass profiles of X-ray galaxy clusters are also successfully fitted for those clusters that are isothermal.

• A fit to the Bullet Cluster 1E0657-56 data can be achieved with the "running" of the gravitational "constant" G without non-baryonic dark matter. The lensing of galaxies and clusters can be explained without dark matter.

• The CMB power spectrum acoustical peaks data including the third peak can be fitted with the density parameters:

$$\Omega_m = \frac{8\pi G_{\rm eff}\rho_m}{3H^2}, \qquad \Omega_G = \frac{\Lambda_G}{H^2}.$$

• The power spectrum for growth of fluctuations and the formation of galaxies and clusters can be incorporated in MOG without dark matter. The acceleration of the universe can be explained in MOG. The universe undergoes a bounce at $t \sim 0$ and the cosmology is singularity-free. The thermodynamic arrow of time is reversed for $t \to -\infty$ and the second law of thermodynamics is not violated as the universe expands away from the bounce towards $t = -\infty$ and $t = +\infty$.

END